nature geoscience

SUPPLEMENTARY INFORMATION

DOI: 10.1038/NGEO2807

Impact of warming on CO_2 emissions from streams countered by aquatic photosynthesis

Benoît O. L. Demars, Gísli M. Gíslason, Jón S. Ólafsson, J. Russell Manson, Nikolai Friberg, James M. Hood, Joshua J. D. Thompson and Thomas E. Freitag

Table of contents

S1. Supplementary methods

Study areas

The present study reports findings from hydrothermal areas of Iceland along the mid-Atlantic ridge between the North American and Eurasian tectonic plates, and Kamchatka sitting atop a small tectonic plate called the Okhotsk block[1,2], at the convergence zone of the Pacific, North American and Eurasian plates.

The natural streams we studied were fed by groundwater from the uppermost permeable rock layer and not by the deep geothermal water, judging from their water chemistry[3]. Heating of the water is indirect and can be very localised, hence cold and hot streams can be found literally metres away from each other's[4].

We organised several summer expeditions to find suitable sites. We worked in seven geothermal fields (Fig S1.1): Hengill and Hveragerdi[3,5], Kerlingarfjöll[6], Hveravellir[7], Torfajökull[8], Vonarskard[9] all from Iceland; and Paratunka[10,11] from Kamchatka, far east Russia (Table S1.1). The geographical coordinates and elevation were compiled in the Supplementary Data table 1 (geography).

All expeditions were constrained by time, weather, the remoteness of the location and the terrain, being a mosaic mountain landscape of ice and hot springs. Hence, fewer sites were sampled in the highlands, but the sites were chosen to spread evenly along the temperature gradient. Four Icelandic geothermal areas (Hengill, Hveragerdi, Torfajökull and Vonarskard) provided enough data (at least 6 sites) spanning a broad temperature range (at least 20°C) to test the effect of temperature within individual geothermal areas. Three sites were excluded from our dataset for different pre-established technical reasons: one site in Hengill had too much lateral inflows as previously reported[4], one site in Kerlingarfjöll's caldera had intermittent turbid water, and one site in Torfajökull had a shorter mean travel time (0.7 min) than the typical response time of the oxygen sensor (95% in 0.75 min). In total we successfully managed to estimate whole stream metabolism at 50 sites, producing the second largest existing individual dataset on stream metabolism across sites[12].

Sites were selected in independent streams, except for two streams in Hveragerdi where it was possible to study cold and warm sections (Table S1.2). The five extra sites represented only 10% of our dataset.

In Iceland, the streams drained areas predominantly covered by moss, grass and protruding volcanic rocks resulting in very little allochthonous organic matter supply to those streams. The lack of trees in the lowland sites was due to long term landscape degradation[13]. In Kamchatka, the streams emerged near the bottom of a hillslope in an alder woodland. Hence, there was more allochthonous organic matter in the Kamchatka streams (small woody debris dams and leaf packs).

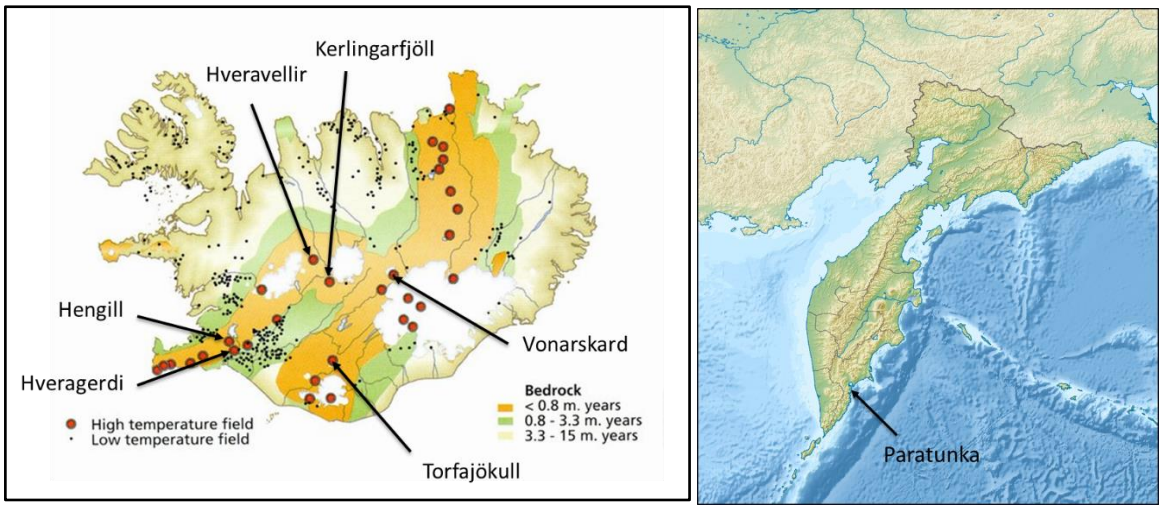

Figure S1.1 | Sampling areas in Iceland and Kamchatka. Maps: Iceland's geothermal fields[14] (Courtesy of National Energy Authority and Ministry of Industries and Innovation) and Kamchatka relief[15] (Courtesy of Nzeemin).

Table S1.1 | Main characteristics of the geothermal areas investigated

Geothermal area (J)	Year(s) of sampling	Number of sites (n)	Temperature range (°C)
*Hengill	2008	13	4.9-25.0
Hveravellir	2011	2	20.8-25.5
Kerlingarfjöll	2011	5	6.4-9.6
*Hveragerdi	2011-2013	13	7.7-45.4
*Torfajökull	2012	6	6.3-37.5
*Vonarskard	2013	7	4.5-33.7
Paratunka	2012	4	6.8-25.7

* areas selected for further analyses in Supplementary Information 6.

Table S1.2 | The two streams with more than one site at Hveragerdi.

sites	Elevation (m)	Temperature (°C)	ΔT† (°C)
STREAM A			
HG 27	285	8.4	
HG 21	104	45.4	37
HG 20	101	36.7	-9
HG 19	98	28.8	-8
HG 18	96	21.9	-7
STREAM B			
HG 23	130	20.6	
HG 22	106	30.4	10

† downstream change in daily average temperature between two sites

Whole stream metabolism

We used a modified two station open diel oxygen method to provide accurate estimates of net ecosystem metabolism (NEP) in heterogeneous streams[4,16,17]. Daily ecosystem respiration (ER) was calculated from the net metabolism at night scaled to 24 hours and daily GPP resulted from subtracting the dark from the light metabolism and averaged over 24 hours. This assumes that ecosystem respiration is the same under daylight and night time. In reality, respiration during daylight is generally (but not always) higher than at night, but this is very much work in progress with method development[18-21]. This assumption has no impact on estimated values of NEP even though the individual magnitudes of GPP and R may be underestimated[22]. Also note, current estimations of respiration during daylight have very large uncertainties and the role of temperature is not yet clear[19-21].

NEP calculations included propagation of uncertainties, including those stemming from small cross-calibration discrepancies and spatial heterogeneity[4,16]. GPP relative uncertainties (interquartile range: 5-35% based on one standard deviation (SD)) were much lower than ER (interquartile range: 51-104% based on one SD). Excel spreadsheets and R code have been made available with example data[16].

GPP and ER were measured in O_2 units and may also be expressed in carbon units (mass O_2=12/32 mass C) using a photosynthetic (PQ) or respiratory quotient (RQ). Here we assumed PQ=RQ=1 in all our conversions[23,24].

We quantified the gas exchange coefficient, discharge, lateral inflows, and mean travel time using tracers (propane, sodium chloride) in all streams, as in our previous study[4]. We used the same equipment and technique as previously reported[4] and only highlight slight departures here. In Kamchatka, we had to rely on a different propane gas supply (5.5 kg Russian commercial gas cylinder) and gas regulator (Donmet, type BPO-5-4DM). We only used the upper half of the gas cylinders and chromatograph analyses from the samples indicated that propane constituted 95-98% of the gas, the remaining was ethane with traces of butane.

Lateral inflows from small tributaries were easily corrected by quantifying discharge by salt dilution gauging and continuously measuring dissolved O_2 with an extra O_2 sensor. Groundwater inflows are however notoriously difficult to characterise and can bias metabolic estimates, especially ecosystem respiration estimates[25,26]. In our case, the correction for lateral inflows[4] had virtually no effect on our results from 2008 and 2011 encompassing 21 sites (linear regression; $ER_{corrected}$=1.03×ER, R^2=0.98, F=3863, P=2.04×10^{-23}, with a regression slope indistinguishable statistically from one with 95% confidence interval: 0.99-1.06). This is because the groundwater dissolved oxygen concentrations were similar to in-stream oxygen concentrations and because we minimised lateral inflows by selecting short reaches with no obvious inflows. Hence, groundwater inflow corrections were not carried out for the remaining sites (2012-2013). In any case, the proportion of lateral inflows

measured across all areas at 45 sites (2008-2013) was completely unrelated to temperature (R^2=0.02, *F*=0.69, *P*=0.41).

We used additional drift free optic oxygen sensors YSI ProODO and 600OMS V2 (YSI Inc., Yellow Springs, OH, USA). The ProODO handheld also provided continuous data on atmospheric pressure, so we did not have to rely on the nearest weather station. The same extreme care was taken to calibrate all the sensors together, cross calibrate pairs of sensors at the field sites, and check calibration at the end (all sensors together). Cross calibration discrepancies did not generally exceed 1-2% dissolved O_2.

The resulting data were made available in the Supplementary Data table 1 (metabolism).

Maximum GPP

GPP_{MAX} is an important parameter to assess light availability (see below, Supplementary Information S2) and convert maximum photosynthesis rates available in the literature to daily estimates of GPP (see below, Supplementary Information S3). The relationship between GPP and photosynthetic active radiation (PAR) was modelled using 5 min time step data with a Michaelis–Menten type equation as follows:

$$GPP = \frac{GPP_{MAX}\ PAR}{k_{PAR} + PAR} \quad \text{(S1)}$$

where GPP_{MAX} is the maximum GPP and k_{PAR} is the PAR at which half the GPP_{MAX} is realised (Fig. S1.2). GPP_{MAX} and k_{PAR} were determined with a nonlinear regression model as previously described[4].

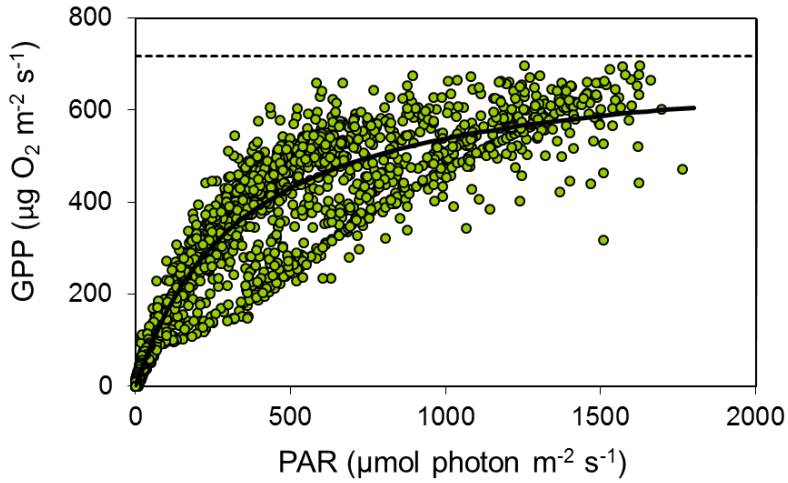

Figure S1.2 | Typical curve of gross primary productivity (GPP) as a function of photosynthetic active radiation (PAR). The black curve is the Michaelis-Menten type equation and the dashed line represents the maximum GPP (GPP_{MAX}) derived from the model. The data are 5 minute time step average from Hengill site 1 (7-15 August 2008). GPP_{MAX}=718 µg O_2 m^{-2} s^{-1}, k_{PAR}=334 µmol m^{-2} s^{-1}.

Steady state

In Iceland, all sites were investigated in August, when daily gross primary production (GPP) and daily ecosystem respiration (ER) rates were found to be constant over several days[4]. Daily ER was strongly dependent on GPP (Fig. S1.3), reflecting the presence of a strong biotic loop[4,27], i.e. balanced nutrient cycling (uptake ≈ regeneration)[28], with faster N and P cycling rates and likely more atmospheric N_2 fixation in the warmer streams preventing nutrient limitation[4,29]. This steady state was clearly not present in Hengill during spring[30] with GPP increasing by about 8% a day at site HEN1 (11.2 °C) in Hengill (under non-limiting light conditions, PAR > 20 mol photon m^{-2} d^{-1}). In Kamchatka, we were fortuitous to find the streams just before leaf emergence (in early June) when photosynthesis is likely to have reached its maximum in this system[31].

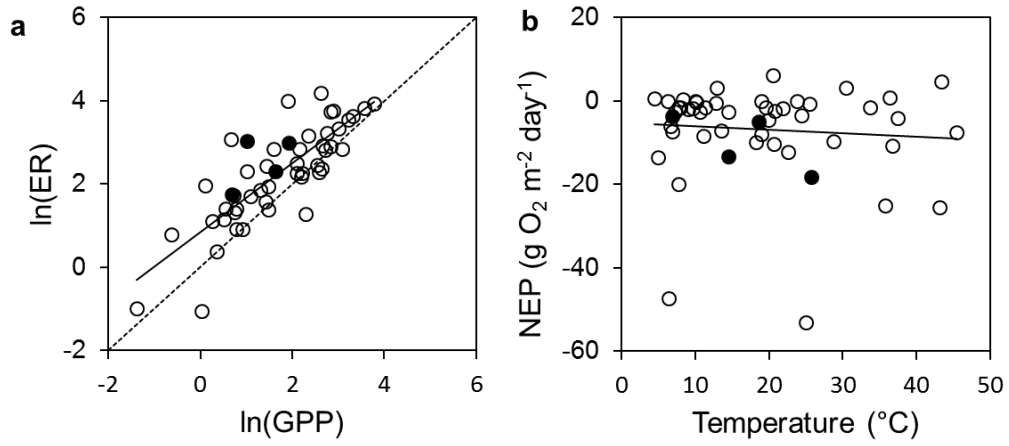

Figure S1.3 | GPP and ER interdependence independent of temperature. a. Ecosystem respiration (ER, in g O_2 m^{-2} day^{-1}) dependence on gross primary productivity (GPP in g O_2 m^{-2} day^{-1}) suggests the presence of a strong microbial biotic loop under steady state conditions, using data from all geothermal areas (R^2=0.66, $F_{1,48}$=92, P=9.4×10^{-13}). The slope (±SE) of the model (0.83±0.09) was close to the expected 1:1 relationship in streams with little allochthonous organic carbon inputs. **b.** Net ecosystem production (±SE) is unrelated to temperature, and averages -6.5 ±1.7 g O_2 m^{-2} day^{-1} at 15°C (R^2=0.008, $F_{1,48}$=0.37, P=0.54). Filled symbols indicate the Kamchatka sites.

Environmental protection

In order to protect the wild fresh water fish stocks against infectious disease agents, or contamination of the environment, all the equipment going in water was disinfected with a solution of 1% by weight (10g/L) of Virkon for 30 minutes, prior to and after deployment in all expeditions.

S2. Temperature and potential confounding effects

It is always difficult to isolate the effect of one factor on a single response variable in the wild. The effect of temperature on photosynthesis is no exception[16]. Here we selected the widest possible temperature gradient and we searched for replicability across geothermal areas with different environmental conditions. Where necessary, we applied logarithmic transformations to normalise the data and minimise heteroscedasticity. The residuals of the fitted models were also visually inspected. Values under detection limits were changed to half the detection limits for the statistical analyses. Note the *P* values were not adjusted for the multiple comparisons between temperature and other abiotic and biotic factors. This only made it harder to reject a possible relationship between temperature and another factor, because some significant relationships may arise by chance alone.

Light availability

All our sites received a minimum daily 24 hour average of 10 mol photon m^{-2} day^{-1} of photosynthetic active radiations (PAR), above which daily GPP was not light limited. Maximum photosynthesis ln(GPP_{max}) was strongly related (R^2=0.95, $F_{1,40}$=950, P=9.7×10^{-34}) to daily photosynthesis ln(GPP_{obs}) across geothermal areas at the 42 sites for which the R^2 of the Michaelis Menten model (Fig. S1.2) exceeded 0.8, demonstrating that slight different light availability (cloud cover) between days did not affect daily GPP differently across sites. The rate of average daily PAR was unrelated to mean daily temperature (R^2<0.01, $F_{1,48}$=0.15, P=0.70).

Water chemistry and nutrient supply

Water samples were collected and filtered with Millipore 0.45 µm pore size on the last day of field work, stored cool or frozen, and analysed at the James Hutton Institute as in previous studies[4,32]. Alkalinity followed the UK standard method[33]. The pH and conductivity were measured in-situ with portable meter (YSI600xlm and YSI 60, Yellow Springs, Ohio). It took a longer time to get a stable reading of pH at sites with low conductivity (30 min). Since our streams had very low DOC and relatively high pH (96% of our sites had pH>6), the excess partial pressure of dissolved carbon dioxide (EpCO_2) could be calculated from alkalinity, pH and temperature according to the empirical formulae[34]:

$$EpCO_2 = \frac{(0.95 \times Alk_{Gran} + 10^{6-pH} + 10^{6+pH-pK_{water}}) \times 10^{6-pH}}{(6.46 - 0.0636 \times T) \times (1 + 2.38 \times 10^{pH-pK_2})} \quad \text{(S2)}$$

$$pK_{water} = -6.0843 + \frac{4471.33}{(273+T)} + 0.017053 \times (273+T) \quad \text{(S3)}$$

$$pK_2 = -6.498 + \frac{2902.39}{(273+T)} + 0.02379 \times (273+T) \quad \text{(S4)}$$

The coefficient 0.95 represented the average factor converting chemical concentration of monovalent ions into chemical activities, T was temperature (°C), Alk_{Gran} was Gran alkalinity (µeq HCO_3 L^{-1}, at pH=4.5), pK_{water} and pK_2 were minus the logarithm of the equilibrium constants for the dissociation of water $[H^+][OH^-]$ and $[H^+]\,[CO_3^-]/[HCO_3^-]$ equilibrium, respectively. The pCO_2 for the atmosphere, $pCO_{2(atm)}$, was set to $10^{-3.5}$ atm (=316 ppm). We applied corrections to take into account elevation[34] and more recent estimate of atmospheric pCO_2 (we used $10^{-3.41}$ atm = 389 ppm). We checked that the above model was valid for our temperature range (0-50°C). Importantly, at the 39 sites for which we had data, log transformed pCO_2 was completely unrelated to temperature (R^2<0.01, $F_{1,37}$=0.16, *P*=0.69) and alkalinity was only very weakly positively related to temperature (R^2=0.16, $F_{1,37}$=7.1, *P*=0.01).

Biogeochemical weathering of rocks increases with temperature. Hence, there was a general tendency for electric conductivity (EC, µS cm^{-1} at 25°C) to increase with temperature (R^2=0.26, $F_{1,48}$=17.2, *P*=0.0001) but importantly this relationship did not hold in half of the geothermal areas and ln(GPP) was only very weakly related to EC (R^2=0.11, $F_{1,48}$=5.9, *P*=0.02). The natural logarithm of Si and K were the most strongly positively related to temperature (R^2=0.50, $F_{1,48}$=48.4, *P*=8.5×10^{-9} and R^2=0.42, $F_{1,48}$=34.3, *P*=4.2×10^{-7}, respectively) but with concentrations above 3.4 mg Si L^{-1} and 0.3 mg K L^{-1}, they cannot be thought as causal factors to explain observed GPP. Nitrogen and phosphorus concentrations were however extremely low at some sites (under limit of detection), but the natural logarithm of total dissolved N and total dissolved P concentrations were unrelated to temperature (R^2<0.01, $F_{1,48}$=0.03, *P*=0.86 and R^2=0.04, $F_{1,48}$=2.0, *P*=0.16, respectively). Other factors such as pH and ln transformed dissolved organic carbon concentration were also barely positively related to temperature (R^2=0.08, $F_{1,48}$=4.5, *P*=0.04; R^2=0.10, $F_{1,48}$=5.3, *P*=0.03 respectively). Overall, water chemistry should not confound our results based on our 50 sites.

Since GPP increases with temperature independently of external nutrient supply, it suggests that, under steady state, in-stream nutrient recycling is the dominant mechanism of nutrient supply to the primary producers via a tight biotic loop (uptake ≈ regeneration)[28]. The strong dependence of daily ecosystem respiration (ER) on daily GPP (R^2 = 0.80, $F_{1,37}$=152, *P*=1.2×10^{-14}; Fig. S1.2) also support this conclusion.

The raw data were made available in the Supplementary Data table 1 (water chemistry).

Hydrology

Although all the streams investigated were groundwater fed, some are more affected than others by winter/spring snow melt and rain on snow events. The sites were accordingly divided under two categories: year round stable hydrology (large spring coming out of the hillslope) and stream susceptible to peak flows (streams draining a small catchment area). Hydrological categories were not related to temperature (logistic regression, z=0.59, *P*=0.56). The Arrhenius mixed model was not significantly improved by adding hydrology as

an extra predictive variable (likelihood ratio test; $\chi_1^2 = 0.07$, *P*=0.79). Hence, hydrology should not confound our results.

The raw data were made available in the Supplementary Data table 1 (hydrology).

Hydraulics

Hyporheic flows in gravel bed and the three dimensional architecture of macrophyte patches and biofilm are known to cause water transient storage zones (streamwater detained in quiescent zones) increasing exchange area and ecological processes[35-37]. It was possible to derive water transient storage (As:A) and storage residence time (Tsto) from our NaCl tracer studies at 32 sites, following the same method used in our preliminary study at Hengill[27]. Neither of these (ln transformed) parameters were related to temperature however (*P*>0.05).

Stream width (w), depth, water velocity, discharge (Q), specific discharge (Q/w) and reaeration rate were not related to temperature (*P*>0.05). Hence, stream hydraulics should not confound our results. The raw data were made available in the Supplementary Data table 1 (hydraulics).

Standing biomass of primary producers and trophic interactions

Food chain length in spring fed streams has been shown to decrease sharply within 35-50°C (Ref.[38]) and trophic interactions across trophic levels can affect standing biomass and GPP of aquatic systems[30,39,40]. In our study, fish were only present at 12 sites in three geothermal areas due to constraints on dispersal (brown trout in Hengill and Hveragerdi; arctic charr in Kerlingarfjöll) within the temperature range 6-22°C at the time of electrofishing. The maximum temperature tolerance for macro-invertebrates in streams is 50°C[38]. In our study, macro-invertebrate density increased with temperature in Hengill[41], and showed a positive trend in Torfajökull (R^2=0.60; $F_{1,4}$=3.07; *P*=0.22) but not in Vonarskard (R^2=0.03; $F_{1,5}$=0.18; *P*=0.69). In Hengill, macrophyte cover and periphyton chlorophyll a biomass were not related to temperature[41], but periphyton chlorophyll a biomass showed positive trends with temperature in Torfajökull (R^2=0.96; $F_{1,4}$=69.5; *P*=0.004) and Vonarskard (R^2=0.47; $F_{1,5}$=4.47; *P*=0.088) in the quasi absence of macrophytes. Note we had no summer data for invertebrate density and periphyton chlorophyll a biomass in Hveragerdi. In Yellowstone National Park, Mushroom spring, in the temperature range 33-68°C, there was no simple correlation between standing biomass (as measured by chlorophyll, protein or RNA per unit area) and photosynthesis[42].

Hence our data suggests that, standing biomass of primary producers, and macroinvertebrate density were not systematically related to temperature. Therefore, the temperature dependence of GPP should not be systematically biased by standing biomass of primary producers and trophic interactions.

S3. Compilation of data from other geothermal areas

In order to compile a dataset of primary productivity spanning the full temperature gradient of photosynthesis in small (1-50 L s^{-1}), comparable streams, we reviewed the literature from geothermal areas, including alkaline hot springs with oxygenic photosynthesis. We selected studies based on direct measurements of oxygen change or the ^{14}C method carried out during summer time.

The first studies were carried out in the mid sixties in Western North America (Fig S3.1): summer 1965 at Drakesbad Thermal Spring in Mount Lassen National Park by Lenn[43] under the direction of Charles Goldman (University of California). This study used the ^{14}C method and reported productivity measurements in g C m^{-2} day^{-1}. The second study was in summer 1966 at Mushroom Spring in Yellowstone National Park by Brock[42] using the same method, but the results were published as radioactive counts per minute per µg chlorophyll per hour. Brock's papers however gave all the necessary details to calculate primary productivity in g C m^{-2} day^{-1} (see below). A third study was also underway at the same time at Ohanapecosh Hot Spring in Mount Rainier by Stockner[44] using the open channel diel oxygen method year round. About two decades later, Revsbech & Ward[45] pioneered the use of the oxygen microprofile method at Octopus Spring in Yellowstone National Park. We also included the oxygenic photosynthesis of two microbial mats with low sulphide concentrations[46] in hot springs from Hveragerdi geothermal area (Iceland) by Jørgensen & Nelson[47], also using the oxygen microprofile approach. Winter primary production using the ^{14}C method were also available for Iceland[48] (Hveragerdi) and may be used for comparative purpose, bearing in mind that those estimates were limited by light availability and therefore not included in our synthesis.

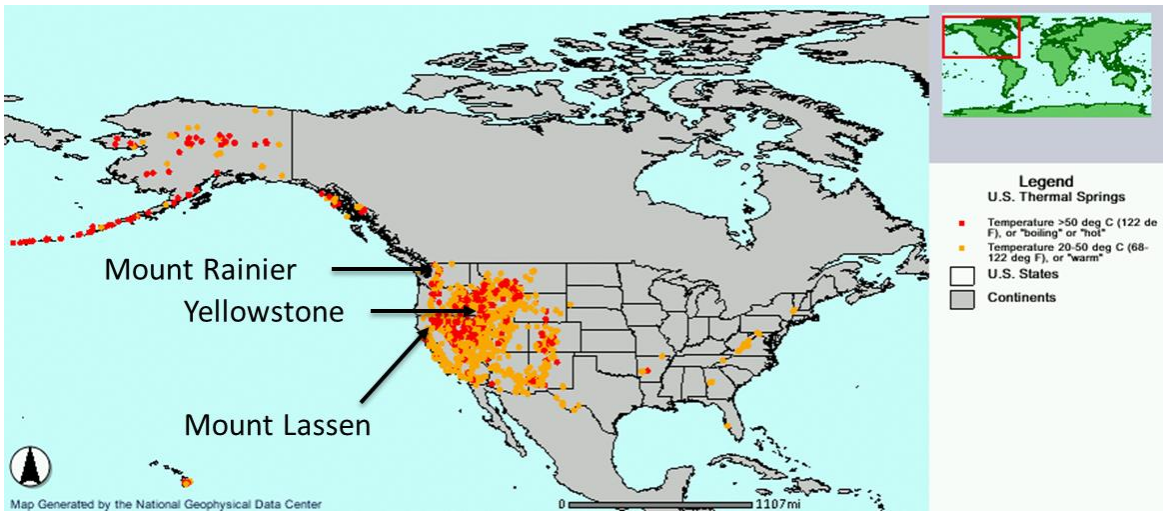

Figure S3.1 | Sampling areas in northern America. Map: United States thermal springs (Courtesy of NOAA National Centers for Environmental Information).

The ^{14}C method with short incubation time in vial gave comparable (≈30% lower) estimates to in-situ ^{14}C and oxygen microprofile methods[45,49]. Among other possibilities, the ^{14}C method estimate is probably more in between net and gross production[50] (this is still debated[51]). In any case, for our purposes, the discrepancy between methods appeared relatively insignificant compared to the one order of magnitude (1000%) in the observed range of primary productivity estimates across sites for a given temperature (Fig 1). From microbial mat cell suspension studies using ^{14}C, it was shown that over 80% of the photosynthetically fixed carbon over two hours incubation was incorporated into polysaccharide[52], and a further 10% was excreted as organic carbon (notably glycolate)[53]. This indicates that photorespiration occurs to a small extent under high O_2 concentrations, despite the carbon concentrating mechanism. We assumed all primary productivity estimates represented GPP for simplicity.

The diel studies performed with the ^{14}C method were only based on four or five measurements, hence the daily estimate of primary production could not be very accurate. The ^{14}C method was probably more accurate with the shortest incubation time and highest primary productivity[50]. The oxygen microprofile studies only reported one measurement under light saturated conditions. Since we knew from our own measurements (in g O_2 m^{-2} day^{-1}) that daily GPP and maximum GPP (GPP_{MAX}) were strongly related[4,30], it was possible to derive daily GPP for both the ^{14}C and oxygen microprofile methods as follows (R^2=0.95, $F_{1,48}$=950, P=9.7×10^{-34}):

$$ln(GPP) = 0.9142 \times ln(GPP_{MAX}) - 0.9386 \quad \text{(S5)}$$

This also had the advantage of standardising the GPP data to light availability at the daily scale (equivalent to same day-length).

In Lenn's study we only selected the shortest incubation time at mid-day (11-1 pm) done on 11 June and 16 July 1965 at the three stations as representative of the maximum primary productivity. The values in g C m^{-2} day^{-1} were averaged and converted in g O_2 m^{-2} day^{-1} (using PQ=1), prior to calculation of daily GPP as presented above.

Brock did not take the calculations far enough to obtain values comparable to other studies. Average temperature data were reported in his Table 1. We extracted the ^{14}C uptake data (counts per minute, % station VI) from his figure 1 with Plot Digitizer for Windows. We know the radioactivity in counts per minute at station VI (6 × 10^8 cpm m^{-2}) and counter efficiency[54] (20%). The number of disintegrations per minute (dpm) and unit area (dpm m^{-2}) were calculated as cpm m^{-2} / counter efficiency and equalled 3 × 10^9 dpm m^{-2}. Since 1 microcurie (µCi) is equivalent to 2.22 × 10^6 dpm and time of incubation was 1 hour, the radioactivity from station VI could equally be expressed as 1351 µCi m^{-2} h^{-1}. The ^{14}C assimilated in a sample at station VI was 0.0381 µCi $sample^{-1}$ $hour^{-1}$, knowing the area of microbial mat introduced in the vial (0.0000282 m^2). This allowed the calculation of absolute values (in µCi

sample^{-1} hour^{-1}) of ^{14}C uptake for the other stations from the data given in his figure 1. The ^{14}C available in a vial was 0.1 µCi. The average (spring source and foot) total inorganic carbon was derived from his Table 2 (total carbon minus organic carbon) and used to calculate the pool of available total inorganic carbon (TIC) in the sample vials (0.258 mg C sample^{-1}). From this the assimilated C (primary productivity in g C m^{-2} day^{-1}) was calculated as follows[50]:

$$assimilated\ C = \frac{assimilated\ ^{14}C}{available\ ^{14}C} \times \frac{available\ TIC}{0.0000282} \times \frac{24}{1000} \times 1.05 \qquad \text{(S6)}$$

with 0.0000282 to convert per sample into per m^2 units, 24/1000 to scale time from hour to day and mg to g of carbon, and 1.05 the isotope discrimination factor. The values from his figure 1 were based on numerous determinations and representative of maximum productivity rate (about 2.4 times the daily rates presented in his figure 2). The values in g C m^{-2} day^{-1} were converted in g O_2 m^{-2} day^{-1} (using PQ=1), prior to calculation of daily GPP as presented above.

The study by Stockner was the most straightforward to integrate as it used the same open channel diel oxygen method. We simply averaged his summer daily GPP estimates. The average day-length was similar to that in Iceland and Kamchatka.

The data of figure 5 from Revsbech & Ward were digitised with Plot Digitizer for Windows and the units converted from mmol O_2 m^{-2} h^{-1} to g O_2 m^{-2} day^{-1}. These values represented maximum activities and were converted to daily GPP as above.

Finally the oxygen microprofile data of figure 4 in Jørgensen & Nelson were integrated to provide the rate of oxygenic photosynthesis in g O_2 m^{-2} day^{-1}. These maximum rates were converted into daily GPP as above.

The resulting data are presented in Table S3.1 below. There was an excellent match between our data and the data from the literature (Figure S3.2).

Table S3.1 | Average temperature (T) and daily gross primary productivity derived from the literature.

site	T average °C	GPP g O_2 m^{-2} day^{-1}	GPP g C m^{-2} day^{-1}
Lenn, 1966			
Station 9	59.0	15.4	5.8
Station 14	55.9	14.5	5.4
Station 19	53.6	14.4	5.4
Brock, 1967			
II	68.1	23.2	8.7
III1/2	65.0	27.2	10.2
VI	58.5	57.4	21.5
VII 3/8	48.3	57.4	21.5
VIII	45.0	43.7	16.4
VII	41.6	51.3	19.3
XI	33.2	24.8	9.3
Stockner, 1968			
Spring 3	37.0	7.9	2.9
Revsbech & Ward 1984			
Octopus1	38.0	7.4	2.8
Octopus2	48.0	4.8	1.8
Octopus3	55.0	9.6	3.6
Octopus4	61.0	9.0	3.4
Octopus5	66.0	6.0	2.2
Octopus6	70.0	3.8	1.4
Jørgensen & Nelson 1988			
mat A	52.0	16.3	6.1
mat B	47.0	9.3	3.5

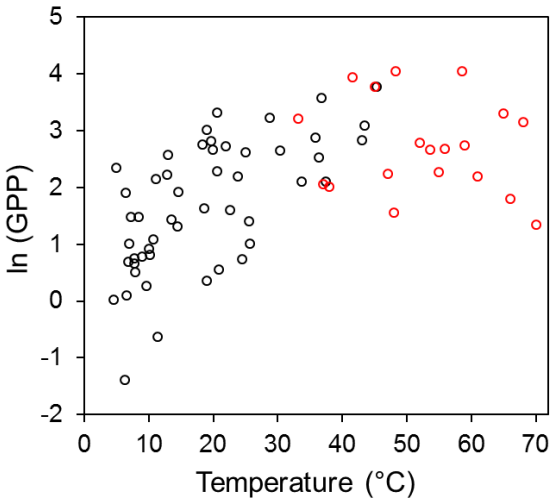

Figure S3.2 | Primary production (GPP in g O_2 m^{-2} day^{-1}) estimates from our study (black circles) and data derived from the literature (red circles). Note the comparability or our data using the open channel diel oxygen method with those from the literature using various methods in the overlapping range 33-45°C.

S4. Thermodynamic theory and fitting with non-linear regression

Three alternative thermodynamic theories[55-57] were investigated using a model assuming a single, rate-limiting 'master reaction' to describe the temperature reaction norm of individual organisms or ecosystem processes. All three theories have been applied to a wide range of organisms and ecosystem processes[58-60]. The Sharpe-Schoolfield theory was the most flexible because independent terms (and parameters) in the denominator captured the decrease in metabolic rates at low and high temperatures. Hence the theory could easily be simplified to produce a more parsimonious model.

The models (Sharpe-Schoolfield and Johnson & Lewin) were fitted using the nonlinear (weighted) least-squares (*nls* function) of the stats package in R statistical software (version 3.1.3)[61]. The 95 percent confidence interval of the parameters was calculated with the function *confint2* using the nlstools package[62] in R. In order to improve heteroscedasticity and normality, model equations were ln transformed and fitted on ln transformed observed GPP (in mg O_2 m^{-2} day^{-1} to avoid negative values). The Sharpe-Schoolfield and Johnson & Lewin models explained the same amount of variability in observed GPP (47%). Visual inspection of residual plots did not reveal any obvious deviations from homoscedasticity or normality. The Johnson & Lewin model was more parsimonious as reflected by a lower AIC than the full model (AIC_{JL}=181.4, AIC_{SS}=184.7) and importantly all parameters were statistically significant (Table S4.1). This was not the case for the full model (Table S4.2).

Our results at high temperature (>45°C) relied on measurements performed in a handful of independent streams (see Supplementary Information 3). Although the choice of the site was driven by marked differences in benthic communities correlated to the temperature change, we re-run the Johnson & Lewin model after down-weighting multiple sites on the same stream by 0.5 (including our sites listed in Table S1.1). The results were very similar (Table S4.3). This, together with the excellent match between our data and the literature data suggested that our results were robust.

The temperature optimum (T_{opt}) of GPP was as previously derived from the Johnson & Lewin model[63]:

$$T_{opt} = \frac{\Delta H_H}{\Delta S_H + R\ ln\left(\frac{\Delta H_H}{\Delta H_A^*} - 1\right)} \quad \text{(S7)}$$

with ΔS_H the difference in entropy of activation between states (normal and high temperatures). In our case, since $\frac{\Delta H_H}{\Delta H_A^*} \approx 2$ (see Table S4.1), then $R\ ln\left(\frac{\Delta H_H}{\Delta H_A^*} - 1\right) \approx 0$, and with $\Delta S_H = \frac{\Delta H_H}{T_H}$ (ref.[55]), we have $T_{opt} \approx T_H$, both temperatures sharing the same standard error. The 68 and 95 percent confidence interval (CI) were calculated by adding to T_{opt} the product of the standard error × Student's *t* critical value at α=0.32 and α=0.05 in both tails of the distribution for 65 degrees of freedom, that is $t_{.32[65]}$ = ±1.002 and $t_{.05[65]}$ = ±1.997, respectively. The temperature optimum of GPP was 45°C, likely within 33-57°C (68% CI), and very likely within 21-70°C (95% CI).

Table S4.1 | Johnson & Lewin model results

parameters	units	initial	fitted	Std. Error	t value	Pr(>|t|)
GPP_{T_C}	mg O_2 m^{-2} day^{-1}	15000	19946.86	9642.80	2.069	0.042568
ΔH_A^*	J mol^{-1}	48200	52026.92	14985.98	3.472	0.000924
ΔH_H	J mol^{-1}	125000	103483.02	32688.23	3.166	0.002355
T_H	K	320	318.06	12.33	25.796	< 2e-16

Table S4.2 | Sharpe-Schoolfield model results

parameters	units	initial	fitted	Std. Error	t value	Pr(>|t|)
GPP_{T_C}	mg O_2 m^{-2} day^{-1}	15000	14805.21	6688.02	2.214	0.0305
ΔH_A^*	J mol^{-1}	48200	22549.00	53261.51	0.423	0.6735
ΔH_L	J mol^{-1}	-138000	-93329.39	149653.92	-0.624	0.5351
T_L	K	283	283.05	32.56	8.694	2.19e-12
ΔH_H	J mol^{-1}	125000	145750.55	151437.76	0.962	0.3395
T_H	K	320	333.79	20.23	16.500	< 2e-16

Table S4.3 | Weighted Johnson & Lewin model results

parameters	units	initial	fitted	Std. Error	t value	Pr(>|t|)
GPP_{T_C}	mg O_2 m^{-2} day^{-1}	15000	20717.97	14461.15	1.433	0.15675
ΔH_A^*	J mol^{-1}	48200	53179.24	19552.76	2.720	0.00837
ΔH_H	J mol^{-1}	125000	88833.26	31927.52	2.782	0.00706
T_H	K	320	314.72	17.75	17.729	< 2e-16

S5. Theoretical assumptions and prediction of the activation energy of GPP

We have made an important theoretical distinction with previous papers regarding the assumption of adaptation. Natural selection is assumed here to operate at the level of the genes, where enzymes evolved with different forms, each fully adapted to a different temperature and performing the same function. This was well expounded in the introduction of *Life Ascending*[64] and has continued to gain further empirical evidence. This allows the prediction of a very wide physiological temperature range for our key enzyme Rubisco, and together with a recent synthesis on the temperature sensitivity of Rubisco, to predict individual and ecosystem behaviours (see below and Figure S5.1). This contrasts with the most recent synthesis where natural selection was assumed to operate at the level of the individual[65].

We provide novel predictions with explicit assumptions based on our current knowledge of Rubisco and the Sharpe-Schoolfield thermodynamic model. The different forms of Rubisco[66,67] are evolutionary adapted to temperature[68,69], i.e. they have different temperature optima (thermal stability) and near perfect optimisation of CO_2 fixation, similarly to other key enzymes such as citrate synthase which catalyses the first reaction in the Krebs' cycle[70]. At the community level, this allows Rubisco carboxylase to be active across a broad temperature range (Fig. S5.1a). The activation energy of Rubisco carboxylase activity among phylogenetic groups was shown to be neither related to the optimum of Rubisco carboxylase activity or the species optimum growth temperature[68]. Hence the average activation energy of Rubisco may be independent of the thermal stability of the molecular scaffolding and more dependent on the molecular mechanisms affecting catalysis at the active site (which is genetically conserved among photosynthesisers across forms of Rubisco[66]). We suggest that natural selection operates mostly on the thermal stability of Rubisco via differences in individual peak performance of photosynthesis, increasing systematically with temperature according to the average activation energy of Rubisco (Fig. S5.1b). Essentially, we assume no temperature compensation in the carboxylation reaction. This is a necessary condition to link the average activation energy of Rubisco to the temperature sensitivity of photosynthesis at the ecosystem level. Alternatively, full temperature compensation would be manifested by a lack of photosynthesis response to temperature at ecosystem scale. The sum of individual thermal responses yield the temperature reaction norm of photosynthesis for aquatic autotrophs at the community level (Fig. S5.1b), providing that Rubisco density and community size structure and biomass are equivalent along the temperature gradient[71].

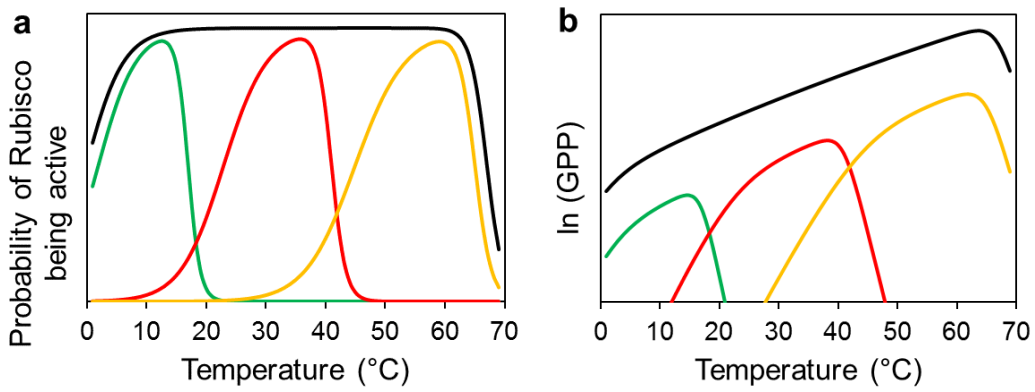

Figure S5.1 | Thermal response of Rubisco activity and gross primary production (GPP) modelled with the Sharpe-Schoolfield theory. a. Expected probability of activity of the different forms of Rubisco (coloured curves) evolutionary adapted to temperature and at community level (black curve). **b.** Expected peak performance of GPP of individual forms of Rubisco (coloured curves) increases systematically with temperature according to the average activation energy of Rubisco carboxylase activity (0.57 eV). The sum of individual thermal responses yields the temperature reaction norm of photosynthesis for aquatic autotrophs at the community level (black line).

S6. Arrhenius linear mixed model

The numerator of the Sharpe-Schoofield theory is Eyring's equation, derived from transition state theory, which is analogous to the Arrhenius equation, derived from collision theory of reaction rates, used in the metabolic theory of ecology (MTE)[72,73]. It suffices to eliminate the leading temperature factor (T/T_c) and replace ΔH_A^* by the activation energy *E* (J mol^{-1}). Since ΔH_A^* is determined at or near T_c, ΔH_A^* is very nearly the same as *E*, with $E = \Delta H_A^* + RT$, as previously derived[74]. Recent MTE papers have also generally expressed *E* in unit of energy per particle (eV) rather than per mole (1 eV=96.4 kJ mol^{-1}) and replaced accordingly the gas constant *R* by the Boltzmann constant *k*=8.62 10^{-5} eV K^{-1}.

The linear mixed model analyses follow previous modelling strategy and recommendations[71,75-77] using the *lmer* function in the lme4 package (version 1.1-10)[77] of R statistical software (version 3.1.3)[61]. The analysis consisted of three steps. The first step was the identification of the most parsimonious structure for the random effects associated with the intercept and slope of the model. The random models were fitted using restricted maximum likelihood (REML) and AIC tests were used to compare models. The second step was to fit the full Arrhenius model using maximum likelihood and test its significance relative to the most parsimonious random model with a likelihood ratio test. Finally, in the third step, the full model was refitted using REML and individual parameters were tested using the lmerTest package (version 2.0-29)[78] in R. Fixed effects were tested with t-tests via Satterthwaite approximations to degrees of freedom. Random effects were tested with likelihood ratio tests (function *rand*)[78]. We also performed a backward elimination of non-significant effects, starting from the random effects, and then fixed effects using the *step* function in lmerTest[78]. The 95% confidence intervals of the parameters of the final (simplified) model were determined by computing a likelihood profile and finding the appropriate cut-offs based on the likelihood ratio test with the function *confint.merMod* from the lme4 package[77]. Finally, the fit of the models was assessed with the conditional and marginal coefficient of determination (R^2) using the R function *r.squaredGLMM* from the MuMIn package[79,80]. The conditional R^2 represents the variance explained by fixed and random factors together; and the marginal R^2 represents the variance explained solely by the fixed effects.

The best (lowest AIC) random structure for the full Arrhenius model included area-specific random deviations ε_E^j and ε_{GPP}^j associated with the slope $\overline{E_a}$ and intercept $\overline{ln(GPP_{T_C})}$ of the overall model, n=39 sites (Table S6.1). The effect of standardised inverse temperature was highly significant given those random effects (likelihood ratio test; $\chi_1^2 = 9.2$, *P* = 0.002). One parameter, the area-specific estimates of the activation energy ε_E^j, was not significant however after backward elimination (likelihood ratio test; $\chi_1^2 = 2.7$, *P* = 0.26) and so the full model could be simplified (Table S6.2). These analyses gave us $\overline{E_a}$ and $ln(GPP_{T_C})$ for each of the four geothermal areas, as well as an overall global estimate for all geothermal areas

combined (Table S6.3). Visual inspections of residual plots did not reveal any obvious deviations from homoscedasticity or normality.

The key findings coming out of these data analyses is that the final model supports a unique apparent activation energy for photosynthesis at 0.50 eV which is within the range of the apparent activation energy of the respiratory complex reported in previous studies (0.47-0.65 eV). The 95% confidence interval (0.35-0.65 eV) also excluded the activation energy of C3 terrestrial plant photosynthesis (0.32 eV), similarly to (and more decisively than) the non-linear Johnson & Lewin model (see main text) and as predicted from our theory.

Table S6.1 | Mixed-effects analysis of data from all four Iceland geothermal areas combined. Models R1 and R2 were fitted using restricted maximum likelihood (REML) and AIC tests were used to compare models. Model F1 was fitted using maximum likelihood and likelihood ratio tests were used to determine the significance of model parameters by comparing the full model (F1) to the most parsimonious restricted model (R2).

Models		df	AIC	logLik	χ^2	*P*
Random effects structure						
R1	$ln\left(GPP_{T_C}\right) * area$	3	120.8			
R2	$E_a * area + ln\left(GPP_{T_C}\right) * area$	5	101.1			
Fixed effects structure (given random structure=R2)						
F1	$\left(\frac{1}{kT_C} - \frac{1}{kT}\right)$ | R2	6	93.9	-41.0	9.2	0.002

df = degree of freedom, AIC = Akaike Information Criteria

Table S6.2 | Parameter estimation and associated probabilities of the full Arrhenius mixed-effects model and the simplified model where ε_E^j was removed following backward elimination. The final simplified model gave a strong conditional R^2=0.74 (variance explained by fixed and random factors), and robust marginal R^2=0.38 (variance explained by fixed factors alone).

	Full model			Simplified model			
parameters	estimates	$test_{df}$	*P* value	estimates	$test_{df}$	*P* value	95% CI
$\overline{E_a}$	0.53	$t_{3.2}$ = 5.2	0.012	0.50	$t_{35.0}$ = 6.7	9×10^{-8}	0.35-0.65
ε_E^j	NA	$\chi_2^2 = 2.6$	0.26	NA	NA	NA	NA
$\overline{ln\left(GPP_{T_C}\right)}$	1.70	$t_{2.95}$ = 4.2	0.025	1.70	$t_{2.97}$ = 4.3	0.024	0.82-2.55
ε_{GPP}^j	NA	$\chi_1^2 = 16.9$	4×10^{-5}	NA	$\chi_1^2 = 16.9$	4×10^{-5}	0.32-1.66

NA = not applicable, CI = confidence interval, df = degrees of freedom

Table S6.3 | Simplified model (i.e. without ε_E^j) refitted using REML to provide estimates of the parameters used to characterize the temperature sensitivity of ecosystem photosynthesis (gross primary production, GPP) for four Icelandic geothermal areas. The model gave a strong conditional R^2=0.74 (variance explained by fixed and random factors), and robust marginal R^2=0.38 (variance explained by fixed factors alone). The *P* value was determined by anova table of type III with Satterthwaite approximation for degrees of freedom. Observed photosynthesis $ln(GPP_{obs})$ was linearly regressed (using ordinary least square regression) against the fitted values of the model $\ln\left(GPP_T^j\right)$ to provide R^2 and *P* values within geothermal areas (with *P* values also significant with a false discovery rate of 0.1, using the Benjamini-Hochberg procedure[81]).

areas	n	$\overline{E_a}$	$\overline{ln\left(GPP_{T_C}\right)}$	ε_{GPP}^j	R^2	$F_{ndf,ddf}$	*P*-value
Hengill	13	0.50	1.70	+0.71	0.33	$F_{1,11}$ = 5.5	0.039
Hveragerdi	13	0.50	1.70	+0.48	0.69	$F_{1,11}$ = 25.0	4×10^{-4}
Torfajökull	6	0.50	1.70	-0.83	0.78	$F_{1,4}$ = 14.4	0.019
Vonarskard	7	0.50	1.70	-0.38	0.62	$F_{1,5}$ = 8.2	0.035
	n	$\overline{E_a}$ ± se	$\overline{ln\left(GPP_{T_C}\right)}$ ± se	cR^2	mR^2	$F_{ndf,ddf}$	*P*-value
all areas	39	0.50 ± 0.07	1.70 ± 0.39	0.38	0.74	$F_{1,35}$ = 45.3	9×10^{-8}

se = standard error, cR^2 = conditional R^2, mR^2 = marginal R^2

ndf, ddf = numerator and denominator degrees of freedom, respectively

S7. The metabolic balance of streams and rivers

The activation energy of photosynthesis and autotrophic respiration are equal[82]. The activation energy of heterotrophic respiration is more complicated however if the activation energy of autotrophic and heterotrophic respiration differs[71,83]. Ecosystem respiration can be divided into four components reflecting respiration of different substrates by different organisms[84-86] and grouped into two fractions: (1) respiration constrained by GPP (θGPP, with θ fraction of autotrophic respiration relative to GPP) with activation energy E_a: respiration by autotrophs + respiration by heterotrophs of autochthonously produced labile organic matter; (2) background respiration (BR) with activation energy E_h: respiration by heterotrophs of autochthonously produced recalcitrant organic matter + respiration by heterotrophs of allochthonous terrestrial organic matter. We express net primary production (*NPP*) as $NPP = (1-\theta)GPP$ [71]. Hence, total ecosystem respiration (*ER*) can be expressed as $ER = \theta\ GPP + BR$ and the net ecosystem production for a given temperature *T* as $NEP_T = GPP_T - ER_T = NPP_T - BR_T$. Now, if the activation energies coupled to *NPP* and *BR* were statistically different ($E_a \neq E_h$, respectively), then we would have:

$$NPP_T = (1-\theta)GPP_{T_C} exp\left[E_a\left(\frac{1}{kT_C} - \frac{1}{kT}\right)\right] \quad \text{(S8)}$$

$$BR_T = \left(ER_{T_C} - \theta\ GPP_{T_C}\right) exp\left[E_h\left(\frac{1}{kT_C} - \frac{1}{kT}\right)\right] \quad \text{(S9)}$$

If, however, $E_a = E_h$ as suggested from our study, we have a much simpler expression for the metabolic balance of aquatic ecosystems with θ cancelling out:

$$NEP_T = \left(GPP_{T_C} - ER_{T_C}\right) exp\left[E\left(\frac{1}{kT_C} - \frac{1}{kT}\right)\right] \quad \text{(S10)}$$

Hence, when ER exceeds GPP (as generally the case for stream ecosystems), net ecosystem production, $NEP_{T_C} = \left(GPP_{T_C} - ER_{T_C}\right)$, simply increases with temperature. Assuming an activation energy of 0.6 eV for both respiration and photosynthesis and existing NEP estimates[87,88], the global CO_2 emissions from the metabolic balance of fluvial networks (streams, rivers and estuaries) would increase by 1.3 times from 0.31 Pg C year^{-1} at 13°C (summer global land surface average temperature[4]) to 0.40 Pg C year^{-1} with a 3°C warming

(land annual mean surface air temperature anomalies for the period 2081-2100 with RCP6.0 scenario[89]). For comparison, our predicted global estimate of CO_2 emissions from the metabolic balance of running waters represents about 14% of the current global terrestrial CO_2 sink[90]. In our groundwater fed streams from geothermal areas, NEP showed no response to temperature, likely because ER was nearly entirely dependent on GPP (Fig. S3.1). This may not be the case for most rivers showing poor correlations between ER and GPP[86].

References

1 Pedoja, K., Bourgeois, J., Pinegina, T. & Higman, B. Does Kamchatka belong to North America? An extruding Okhotsk block suggested by coastal neotectonics of the Ozernoi Peninsula, Kamchatka, Russia. *Geology* **34**, 353-356 (2006).

2 Pinegina, T. K. *et al.* A nexus of plate interaction: Vertical deformation of Holocene wave-built terraces on the Kamchatsky Peninsula (Kamchatka, Russia). *Geol. Soc. Am. Bull* **125**, 1554-1568 (2013).

3 Arnason, B., Theodorsson, P., Björnsson, S. & Saemundsson, K. Hengill, a high temperature thermal area in Iceland. *Bulletin Volcanologique* **33**, 245-259 (1969).

4 Demars, B. O. L. *et al.* Temperature and the metabolic balance of streams. *Freshwater Biol.* **56**, 1106-1121 (2011).

5 Zakharova, O. K. & Spichak, V. V. Geothermal fields of Hengill Volcano, Iceland. *Journal of Volcanology and Seismology* **6**, 1-14 (2012).

6 Stevenson, J. A., Gilbert, J. S., McGarvie, D. W. & Smellie, J. L. Explosive rhyolite tuya formation: classic examples from Kerlingarfjoll, Iceland. *Quat. Sci. Rev* **30**, 192-209 (2011).

7 Daba, G. Comparative study on the high-temperature fields of Hveravellir in Iceland and Tendaho in Ethiopia. (United Nations University, Reykjavik, Iceland, 2008).

8 Arnórsson, S., Ívarsson, G., Cuff, K. E. & Sæmundsson, K. Geothermal activity in the Torfajökull field, South Iceland: summary of geochemical studies. *Jökull* **37**, 1-10 (1987).

9 Fridleifsson, G. O. & Johannesson, H. in *Proceedings World Geothermal Congress 2005.* 1-5.

10 Vakin, E. A. *et al.* in *U.N. Symposium on the Devopment and Utilization of Geothermal Resources.* 1116-1133.

11 Leonov, V. L. & Rogozin, A. N. in *Proceedings World Geothermal Congress 2010.* 1-7.

12 Bernot, M. J. *et al.* Inter-regional comparison of land-use effects on stream metabolism. *Freshwater Biol.* **55**, 1874-1890 (2010).

13 Simpson, I. A., Dugmore, A. J., Thomson, A. & Vesteinsson, O. Crossing the thresholds: human ecology and historical patterns of landscape degradation. *Catena* **42**, 175-192 (2001).

14 National Energy Authority and Ministries of Industry and Commerce. Energy in Iceland. Historical Perspective, Present Status, Future Outlook. www.os.is/media/eldri-utgafa/Energy_in_Iceland_2ed_2006.pdf (2006).

15 Nzeemin. *Relief map of Kamchatka*, <https://ru.wikipedia.org/wiki/%D0%A4%D0%B0%D0%B9%D0%BB:Relief_Map_of_Kamchatka_Krai.png> (2012).

16 Demars, B. O. L., Thompson, J. & Manson, J. R. Stream metabolism and the open diel oxygen method: Principles, practice, and perspectives. *Limnol. Oceanogr. Methods* **13**, 356-374 (2015).

17 Odum, H. T. Primary production in flowing waters. *Limnol. Oceanogr* **1**, 102-117 (1956).

18 Haggerty, R., Marti, E., Argerich, A., von Schiller, D. & Grimm, N. B. Resazurin as a "smart'' tracer for quantifying metabolically active transient storage in stream ecosystems. *Journal of Geophysical Research-Biogeosciences* **114**, G03014 (2009).

19 Carvalho, M. C. & Eyre, B. D. Measurement of planktonic CO2 respiration in the light. *Limnol. Oceanogr. Methods* **10**, 167-178 (2012).

20 Hotchkiss, E. R. & Hall, R. O., Jr. High rates of daytime respiration in three streams: Use of delta O-18(O2) and O-2 to model diel ecosystem metabolism. *Limnol. Oceanogr* **59**, 798-810 (2014).

21 Gonzalez-Pinzon, R., Peipoch, M., Haggerty, R., Marti, E. & Fleckenstein, J. H. Nighttime and daytime respiration in a headwater stream. *Ecohydrology* **9**, 93-100 (2016).

22 Staehr, P. A. *et al.* Lake metabolism and the diel oxygen technique: State of the science. *Limnol. Oceanogr. Methods* **8**, 628-644 (2010).

23 Vollenweider, R. A., Talling, J. F. & Westlake, D. F. Vol. IBP Handbook No. 12 (Blackwell Scientific Publication, London, 1969).
24 Williams, P. J. l. B. & del Giorgio, P. A. in *Respiration in aquatic ecosystems* (eds P.A. del Giorgio & P.J. le B. Williams) 1-17 (Oxford University Press, 2005).
25 McCutchan, J. H., Lewis, W. M. & Saunders, I. J. F. Uncertainty in the estimation of stream metabolism from open-channel oxygen concentrations. *J. North Am. Benthol. Soc.* **17**, 155-164 (1998).
26 Hall, R. O. & Tank, J. L. Correcting whole-stream estimates of metabolism for groundwater input. *Limnology and Oceanography: Methods* **3**, 222-229 (2005).
27 Demars, B. O. L., Manson, J. R., Olafsson, J. S., Gislason, G. M. & Friberg, N. Stream hydraulics and temperature determine the metabolism of geothermal Icelandic streams. *Knowledge and Management of Aquatic Ecosystems* **402**, 05 (2011).
28 Brookshire, E. N., Valett, H. M. & Gerber, S. Maintenance of terrestrial nutrient loss signatures during in-stream transport. *Ecology* **90**, 293-299 (2009).
29 Welter, J. R. *et al.* Does N_2 fixation amplify the temperature dependence of ecosystem metabolism? *Ecology* **96**, 603-610 (2015).
30 O'Gorman, E. J. *et al.* Impacts of warming on the structure and functioning of aquatic communities: individual to ecosystem level responses. *Adv. Ecol. Res.* **47**, 81-176 (2012).
31 Roberts, B. J., Mulholland, P. J. & Hill, W. R. Multiple scales of temporal variability in ecosystem metabolism rates: Results from 2 years of continuous monitoring in a forested headwater stream. *Ecosystems* **10**, 588-606 (2007).
32 Demars, B. O. L. & Edwards, A. C. A seasonal survey of surface water habitats within the River Spey basin, Scotland: major nutrient properties. *Aquatic Conservation-Marine and Freshwater Ecosystems* **17**, 565-583 (2007).
33 Standing Committee of Analysts. *The determination of alkalinity and acidity in water*. (HMSO, 1981).
34 Neal, C., House, W. A. & Down, K. An assessment of excess carbon dioxide partial pressures in natural waters based on pH and alkalinity measurements. *The Science of the Total Environment* **210/211**, 173-185 (1998).
35 Ensign, S. H. & Doyle, M. W. In-channel transient storage and associated nutrient retention: Evidence from experimental manipulations. *Limnol. Oceanogr* **50**, 1740-1751 (2005).
36 Battin, T. J., Kaplan, L. A., Newbold, J. D. & Hansen, C. M. E. Contributions of microbial biofilms to ecosystem processes in stream mesocosms. *Nature* **426**, 439-442 (2003).
37 Odum, H. T. Trophic structure and productivity of Silver springs, Florida. *Ecol. Monogr.* **27**, 55-112 (1957).
38 Glazier, D. S. Temperature affects food-chain length and macroinvertebrate species richness in spring ecosystems. *Freshw. Sci.* **31**, 575-585 (2012).
39 Atwood, T. B. *et al.* Predator-induced reduction of freshwater carbon dioxide emissions. *Nat. Geosci.* **6**, 191-194 (2013).
40 Dickman, E. M., Newell, J. M., Gonzalez, M. J. & Vanni, M. J. Light, nutrients, and food-chain length constrain planktonic energy transfer efficiency across multiple trophic levels. *Proc. Natl. Acad. Sci. U. S. A* **105**, 18408-18412 (2008).
41 Friberg, N. *et al.* Relationships between structure and function in streams contrasting in temperature. *Freshwater Biol.* **54**, 2051-2068 (2009).
42 Brock, T. D. Relationship between standing crop and primary productivity along a hot spring thermal gradient. *Ecology* **48**, 566-571 (1967).
43 Lenn, R. C. *Primary productivity of a thermal spring* MSc thesis, University of California Davis, (1966).
44 Stockner, J. G. Algal growth and primary productivity in a thermal stream. *J. Fish Res. Board Can.* **25**, 2037-2058 (1968).

45 Revsbech, N. P. & Ward, D. M. Microelectrode studies of interstitial water chemistry and photosynthetic activity in a hot-spring microbial mat. *Appl. Environ. Microbiol.* **48**, 270-275 (1984).
46 Cohen, Y., Jorgensen, B. B., Revsbech, N. P. & Poplawski, R. Adaptation to hydrogen sulfide of oxygenic and anoxygenic photosynthesis among Cyanobacteria. *Appl. Environ. Microbiol.* **51**, 398-407 (1986).
47 Jorgensen, B. B. & Nelson, D. C. Bacterial zonation, photosynthesis, and spectral light distribution in hot spring microbial mats of Iceland. *Microb. Ecol.* **16**, 133-147 (1988).
48 Sperling, J. A. Algal ecology of southern Icelandic hot springs in winter. *Ecology* **56**, 183-190 (1975).
49 Sperling, J. A. & Hale, G. M. Patterns of radiocarbon uptake by a thermophilic blue-green alga under varying conditions of incubation. *Limnol. Oceanogr* **18**, 658-662 (1973).
50 Peterson, B. J. Aquatic primary productivity and the 14C-CO2 method - a history of the productivity problem. *Annu. Rev. Ecol. Syst.* **11**, 359-385 (1980).
51 Kosten, S., Demars, B. O. L. & Moss, B. Distinguishing autotrophic and heterotrophic respiration based on diel oxygen change curves: revisiting Dr. Faustus. *Freshwater Biol.* **59**, 649-651 (2014).
52 Konopka, A. Accumulation and utilization of polysaccharide by hot spring phototrophs during a light-dark transition. *Fems Microbiology Ecology* **102**, 27-32 (1992).
53 Bateson, M. M. & Ward, D. M. Photoexcretion and fate of glycolate in a hot spring cyanobacterial mat. *Appl. Environ. Microbiol.* **54**, 1738-1743 (1988).
54 Brock, T. D. & Brock, M. L. Measurement of chlorophyll, primary productivity, phosphorylation and macromolecules in benthic algal mats. *Limnol. Oceanogr* **12**, 600-605 (1967).
55 Schoolfield, R. M., Sharpe, P. J. H. & Magnuson, C. E. Non-linear regression of biological temperature dependent rate models based on absolute reaction rate theory. *J. Theor. Biol.* **88**, 719-731 (1981).
56 Ratkowsky, D. A., Olley, J. & Ross, T. Unifying temperature effects on the growth rate of bacteria and the stability of globular proteins. *J. Theor. Biol.* **233**, 351-362 (2005).
57 Hobbs, J. K. *et al.* Change in heat capacity for enzyme catalysis determines temperature dependence of enzyme catalyzed rates. *Acs Chemical Biology* **8**, 2388-2393 (2013).
58 Wagner, T. L., Wu, H. I., Sharpe, P. J. H., Schoolfield, R. M. & Coulson, R. N. Modeling insect development rates. A literature review and application of a biophysical model. *Ann. Entomol. Soc. Am.* **77**, 208-225 (1984).
59 Corkrey, R., Olley, J., Ratkowsky, D., McMeekin, T. & Ross, T. Universality of thermodynamic constants governing biological growth rates. *PLoS. ONE* **7**, e32003 (2012).
60 Schipper, L. A., Hobbs, J. K., Rutledge, S. & Arcus, V. L. Thermodynamic theory explains the temperature optima of soil microbial processes and high Q(10) values at low temperatures. *Glob. Change. Biol* **20**, 3578-3586 (2014).
61 R Core Team. *R: A language and environment for statistical computing. R Foundation for Statistical Computing*, <http://www.R-project.org/> (2015).
62 Baty, F., Delignette-Muller, M.-L., Charles, S., Flandrois, J.-P. & Ritz, C. Package 'nlstools' Tools for Nonlinear Regression Analysis. R package version 1.0-2. <https://CRAN.R-project.org/package=nlstools> (2015).
63 Niinemets, U., Oja, V. & Kull, O. Shape of leaf photosynthetic electron transport versus temperature response curve is not constant along canopy light gradients in temperate deciduous trees. *Plant Cell Environ.* **22**, 1497-1513 (1999).
64 Lane, N. *Life Ascending. The Ten Great Inventions of Evolution*. 344 (Profile books, 2009).
65 Pawar, S., Dell, A. I. & Savage, V. M. in *Aquatic Functional Biodiversity. An Ecological and Evolutionary Perspective* (eds A. Belgrano, G. Woodward, & U. Jacob) Ch. 1, 3-36 (Academic Press, 2015).

66 Tabita, F. R. *et al.* Function, structure, and evolution of the RubisCO-like proteins and their RubisCO homologs. *Microbiol. Mol. Biol. Rev.* **71**, 576-599 (2007).
67 Tabita, F. R., Hanson, T. E., Satagopan, S., Witte, B. H. & Kreel, N. E. Phylogenetic and evolutionary relationships of RubisCO and the RubisCO-like proteins and the functional lessons provided by diverse molecular forms. *Philos. T. Roy. Soc. B* **363**, 2629-2640 (2008).
68 Galmés, J., Kapralov, M. V., Copolovici, L. O., Hermida-Carrera, C. & Niinemets, Ü. Temperature responses of the Rubisco maximum carboxylase activity across domains of life: phylogenetic signals, trade-offs, and importance for carbon gain. *Photosynth. Res* **123**, 183-201 (2015).
69 Tcherkez, G. G. B., Farquhar, G. D. & Andrews, T. J. Despite slow catalysis and confused substrate specificity, all ribulose bisphosphate carboxylases may be nearly perfectly optimized. *Proc. Natl. Acad. Sci. U. S. A* **103**, 7246-7251 (2006).
70 Russell, R. J. M., Gerike, U., Danson, M. J., Hough, D. W. & Taylor, G. L. Structural adaptations of the cold-active citrate synthase from an Antarctic bacterium. *Structure* **6**, 351-361 (1998).
71 Yvon-Durocher, G. *et al.* Reconciling the temperature dependence of respiration across timescales and ecosystem types. *Nature* **487**, 472-476 (2012).
72 Gillooly, J. F., Brown, J. H., West, G. B., Savage, V. M. & Charnov, E. L. Effects of size and temperature on metabolic rate. *Science* **293**, 2248-2251 (2001).
73 Enquist, B. J. *et al.* Scaling metabolism from organisms to ecosystems. *Nature* **423**, 639-642 (2003).
74 Johnson, F. H., Eyring, H. & Stover, B. J. *The Theory of Rate Processes in Biology and Medicine*. (John Wiley & Sons, 1974).
75 Winter, B. Linear models and linear mixed effects models in R with linguistic applications. *arXiv* **1308.5499.**, <http://arxiv.org/pdf/1308.5499.pdf> (2013).
76 Bolker, B. M. *et al.* Generalized linear mixed models: a practical guide for ecology and evolution. *Trends Ecol. Evol* **24**, 127-135 (2009).
77 Bates, D. *et al.* Package 'lme4' Linear Mixed-Effects Models using 'Eigen' and S4. R package version 1.1-10. <https://CRAN.R-project.org/package=lme4> (2015).
78 Kuznetsova, A., Brockhoff, P. B. & Christensen, R. H. B. lmerTest: Tests in Linear Mixed Effects Models. R package version 2.0-29. <http://CRAN.R-project.org/package=lmerTest> (2015).
79 Barton, K. Package 'MuMIn'. R package version 1.15.6. <https://CRAN.R-project.org/package=MuMIn> (2016).
80 Johnson, P. C. D. Extension of Nakagawa & Schielzeth's R-GLMM(2) to random slopes models. *Methods Ecol. Evol.* **5**, 944-946 (2014).
81 Benjamini, Y. & Hochberg, Y. Controlling the false discovery rate - A practical and powerful approach to multiple testing. *J. Roy. Stat. Soc. B Met.* **57**, 289-300 (1995).
82 Allen, A. P., Gillooly, J. F. & Brown, J. H. Linking the global carbon cycle to individual metabolism. *Funct. Ecol* **19**, 202-213 (2005).
83 Yvon-Durocher, G., Jones, J. I., Trimmer, M., Woodward, G. & Montoya, J. M. Warming alters the metabolic balance of ecosystems. *Philos. T. Roy. Soc. B* **365**, 2117-2126 (2010).
84 del Giorgio, P. A. & Williams, P. J. l. B. in *Respiration in aquatic ecosystems* (eds P.A. del Giorgio & P.J. le B. Williams) Ch. 14, 267-303 (Oxford University Press, 2005).
85 Solomon, C. T. *et al.* Ecosystem respiration: Drivers of daily variability and background respiration in lakes around the globe. *Limnol. Oceanogr* **58**, 849-866 (2013).
86 Hall, R. O. & Beaulieu, J. J. Estimating autotrophic respiration in streams using daily metabolism data. *Freshw. Sci.* **32**, 507-516 (2013).
87 Battin, T. J. *et al.* Biophysical controls on organic carbon fluxes in fluvial networks. *Nat. Geosci.* **1**, 95-100 (2008).
88 Battin, T. J. *et al.* Biophysical controls on organic carbon fluxes in fluvial networks (vol 1, pg 95, 2008). *Nat. Geosci.* **2**, 595-595 (2009).

89 Collins, M. *et al.* in *Climate Change 2013: The Physical Science Basis. Contribution of Working Group I to the Fifth Assessment Report of the Intergovernmental Panel on Climate Change* (eds T.F. Stocker *et al.*) Ch. 12, 1029-1136 (Cambridge, United Kingdom and New York, NY, USA, 2013).

90 Le Quéré, C. *et al.* Global carbon budget 2014. *Earth System Science Data* **7**, 47-85 (2015).